Particle Trapping in Arbitrary Trajectories Using First-Order Bessel-Like Acoustic Beams

Xuemei Ren,[1,‡] Qinxin Zhou,[1,‡] Zheng Xu,[1,2,*] and Xiaojun Liu[3,†]

[1] *Institute of Acoustics, Tongji University, Shanghai 200092, China*

[2] *Jiangsu Key Laboratory of Opto-Electronic Technology, School of Physics and Technology, Nanjing Normal University, Nanjing 210023, China*

[3] *Key Laboratory of Modern Acoustics, School of Physics, Nanjing University, Nanjing 210093, China*

(Received 8 September 2020; revised 22 December 2020; accepted 20 April 2021; published 18 May 2021)

In general, singular acoustic beams travel in a straight line and expand during propagation, which limits the scope of their applications. We present a method for generating paraxial zero-order Bessel-like acoustic beams with arbitrary trajectories in water. We then add a vortex phase to obtain a first-order Bessel-like acoustic beam. This beam exhibits a combination of features of vortex, Bessel, and Airy beams. Moreover, it maintains a dark "hole" in the center, preserving its angular momentum, and displays resistance to diffraction, self-healing, and self-bending during propagation. Furthermore, we experimentally realize the beam using a three-dimensionally printed phase mask and observe the acoustic field distribution using the Schlieren imaging method. Finally, we realize particle trapping and transport in a curved trajectory in water.

DOI: 10.1103/PhysRevApplied.15.054041

I. INTRODUCTION

The diffraction-free Bessel beam was first noted as a mathematical construct by Durnin *et al.* in 1987 [1]. A diffraction-free beam has invariance in its lateral and axial intensity profiles as it propagates. When diffraction-free beams pass through a finite aperture, diffraction eventually occurs. The rate of diffraction depends on the size of the aperture relative to the features of the beam [2]. Subsequently, many methods are proposed to generate this beam, for example, using an axicon lens [3–8], a spatial light modulator [9–11], a distributed Bragg reflector [12], or superposing multiple Airy beams [13]. To control the shape of the beam, methods to generate arbitrary-trajectory light beams are proposed that modulate the initial phase of the light source [14–16]. For example, Chremmos *et al.* theoretically proposed a method for generating zero-order Bessel-like optical beams with arbitrary trajectories [14]. Zhao *et al.* experimentally demonstrated self-accelerating Bessel-like optical beams propagating along arbitrary trajectories in free space [15]. They went on to generate first-order Bessel-like optical beams, which they applied for the optical manipulation of microparticles [16]. However, the generation of an arbitrary curve is still a challenge in acoustics.

Owing to the acoustic radiation force, acoustic tweezers can move, separate, and rotate particles without physical contact. Baresch *et al.* demonstrated experimentally the use of single-beam acoustic tweezers to trap solid elastic particles [17,18] and microbubbles [19]. By combining acoustic holography and a phased array, Melde *et al.* realized dynamic particle manipulation by controlling the phase delay of the output beam to guide the position of the projected hologram [20,21]. Norasikin *et al.* presented SoundBender, a hybrid sound modulator that combines the versatility of phased arrays of transducers with the precision of acoustic metamaterials and shows acoustic radiation forces behind obstacles [22]. Minin and co-workers presented an "acoustic hook," which exhibited self-bending and could focus behind obstacles that were directly in the beam path [23–25]. Moreover, the Drinkwater group implemented holographic acoustic tweezers that enabled individual positioning of multiple particles [26–33]. However, phased arrays are relatively expensive and their circuitry is complex. For trapping particles along the direction of beam propagation, Bessel beams [34–39] can be used, which trap particles in the central axis, owing to the negative radiation force along the radial axis.

Here, we generate self-bending zero-order Bessel-like acoustic beams that can follow snakelike, Gaussian, and even three-dimensional (3D) vortex trajectories. The main lobe of such beams remains almost constant during propagation and can even recover itself after being blocked. Then, we superimpose the vortex phase on the beam to

*gotoxvzheng@tongji.edu.cn

†liuxiaojun@nju.edu.cn

‡These authors contributed equally to this work.

generate first-order Bessel-like acoustic beams that have a dark "hole" in their center. We also use Schlieren imaging to verify the acoustic field of the beam and then carry out particle-trapping experiments in a predefined trajectory. The proposed beams are nondiffracting and self-healing. They have symmetric transverse beam profiles, and their curve can be predesigned. The proposed acoustic lens has potential biomedical applications, such as cell transportation in a predefined trajectory and targeted drug delivery *in vivo*.

II. EXPERIMENT

We use the Schlieren imaging method to visualize the acoustic field [40–44]. As shown in Fig. 1, a laser beam (532 nm; DPGL-2150F, Photop, China) is expanded to form a collimated light beam with a diameter of 75 mm using lenses $L1$ and $L2$ that is incident on the acoustic field. The acoustic field is generated in a transparent rectangular water tank made from quartz glass with dimensions of $100 \times 200 \times 200$ mm^3 (width × length × height). The rear surface of the tank is placed at the front focal plane of lens $L3$ to serve as the object plane, and the upper surface of the water tank is open. To visualize the acoustic field, a circular plate that blocks the zero-order diffraction light is placed in the transform plane. An intensified charge-coupled device camera (iStar DH734-18U-03, Andor, UK) is placed at the imaging plane to record the images. A plane-wave field is generated by an ultrasonic transducer (DYW-2M-01T, Dayu Electric, China), which has a radius and center frequency of 25 mm and 2 MHz, respectively. The acoustic lens (photosensitive resin, 1160 kg/m^3, 2.6 GPa, 0.43) is bonded to the surface of the transducer plate using a coupling material and immersed in water. To create traveling waves, the absorber is placed at the bottom of the water tank. The distance between the transducer and the absorber is 120 mm. The transducer is driven by a signal generator (AFG3021, Tektronix) and a power amplifier (ATA-122D, Aigtek, China). To image the particle trajectory, a digital single lens reflex is used. The camera body is a Nikon D800 and the camera lens is a Sigma 105 mm F2.8 EX DG Macro OS. The distribution of the acoustic field is measured by a hydrophone (NH0200, Precision Acoustics, UK) with a preamplifier (DCPS0035, Precision Acoustics, UK).

III. THEORY

A. Generation of the first-order Bessel-like acoustic beam

The method to generate the curved Bessel beam is based on a modification of the conical ray pattern of standard Bessel beams to create deformed ray cones that converge along a prespecified focal line. We first perform a numerical calculation to configure the initial phase (i.e., to generate a curved zero-order Bessel-like acoustic beam); the working frequency of the incident acoustic plane wave is 2 MHz. The angular spectrum method is the main simulation tool used to construct the acoustic field for different initial phases.

In the paraxial regime, the Fresnel integral is [14]

$$u(x,y,z) = \iint \frac{u(X,Y,0)}{2\pi iz} e^{i\{[(X-x)^2+(Y-y)^2]/2z\}} dXdY, \quad (1)$$

where $u(X,Y,0) = A(X,Y)\exp[iQ(X,Y)]$ is the phase-modulated input wave front with the transverse and longitudinal coordinates being scaled by l and kl^2, respectively; k is the wave number; l is an arbitrary length; and Q is a specifically designed phase that enables the zero-order Bessel-like acoustic beam to propagate along a predefined curved trajectory defined by $[f(z), g(z), z]$ in free space. Under the paraxial and slowly varying envelope approximations, the beam structure at input $z = 0$ is given by [15]

$$u(X,Y) = \exp\left(-\frac{X^2+Y^2}{w^2}\right)\exp[iQ(X,Y)], \quad (2)$$

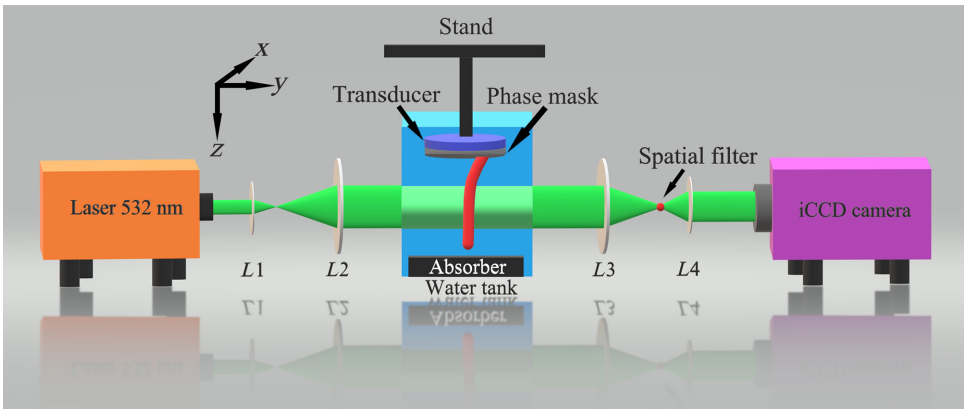

FIG. 1. Schematic diagram of the experimental setup for Schlieren imaging.

where w is the characteristic beam size and $Q(X, Y)$ is determined by

$$Q(X,Y) = \frac{k_0}{2}\int_0^Z \left\{[f'(\zeta)]^2 + [g'(\zeta)]^2 - \left(\frac{\beta}{k_0}\right)^2\right\}d\zeta - k_0\frac{(f-X)^2+(g-Y)^2}{2z}, \quad (3)$$

$$\frac{\beta^2 z^2}{k_0^2} = [X - f(z) + zf'(z)]^2 + [Y - g(z) + zg'(z)]^2, \quad (4)$$

where k_0 and β are the free-space and transverse wave numbers, respectively. Through Eqs. (3) and (4), Q can be determined, and one of the phase distributions for a specified curve is shown as Fig. 2(a).

The specific process for generating the first-order Bessel-like acoustic beam phase as it passes through the phase lens is illustrated in Fig. 2. The zero-order Bessel-like acoustic beam phase and the vortex phase are shown in Figs. 2(a) and 2(b), respectively. From the superposition of these two phases, and limiting the beam using a circular aperture because of the finite size of the acoustic source [Fig. 2(c)], the first-order Bessel-like acoustic beam phase in Fig. 2(d) is finally produced at the radiation surface. The phase map [Fig. 2(d)] is rendered into a 3D-printed transmission element, the material of which has a speed of sound different from that of water. In fabricating the acoustic lens, we assume one-dimensional propagation inside the thin element and neglect shear waves and attenuation, such that the phase lag of each pixel of the lens is proportional to its thickness [20]. The acoustic lens is bonded to the surface of the transducer plate and planar acoustic waves are modified to generate the designed phase profile.

B. Acoustic radiation force

In a fluid, particles are subjected to the acoustic radiation force from the scattering of ultrasound waves from the particles [45]. The acoustic radiation force, $\vec{F}_{\text{rad}}(\vec{r})$, exerted on a Rayleigh particle can be expressed in terms of pressure, $p(\vec{r}, t)$, as [46]

$$\vec{F}_{\text{rad}}(\vec{r}) = \frac{1}{2}\text{Re}[\alpha_a p\nabla p^* + \beta_a k^{-2}(\nabla p\cdot\nabla)\nabla p^*], \quad (5)$$

where the coefficients α_a and β_a represent dipole and quadrupole polarizabilities, respectively; and $k = \omega/c_m$ is the wave number, where ω is the angular frequency of the incident acoustic plane wave and c_m is the speed of sound in the medium. The coefficients α_a and β_a are given by

$$\alpha_a = \frac{4\pi a_p^3}{3\rho_m c_m^2} f_0\left[-1 + i\frac{1}{3}(f_0 + f_1)(ka_p)^3\right], \quad (5a)$$

$$\beta_a = \frac{2\pi a_p^3}{\rho_m c_m^2} f_1\left[1 + i\frac{1}{6}f_1(ka_p)^3\right], \quad (5b)$$

where the monopole coupling coefficient, f_0, and the dipole coupling coefficient, f_1, are given by

$$f_0 = 1 - \frac{\rho_m c_m^2}{\rho_p c_p^2}, \quad (5c)$$

$$f_1 = 2\frac{\rho_p - \rho_m}{2\rho_p + \rho_m}. \quad (5d)$$

Here, a_p, ρ_p, and c_p represent the radius of the particle (35 μm), the density of the particle (1080 kg/m^3), and the speed of sound in the particle (2350 m/s), respectively. In Eq. (5), ρ_m and c_m represent the density of the medium (998 kg/m^3) and the speed of sound in the medium (1482 m/s), respectively. For a suspended Rayleigh particle in an ideal fluid, the acoustic radiation force can trap heavy particles into positions at which the acoustic intensity is near zero (i.e., when the relationship between the particle density and fluid density meets the condition that the acoustic contrast factor is greater than zero). Therefore, heavy particles can be trapped in a dark hole and move along the predefined trajectory.

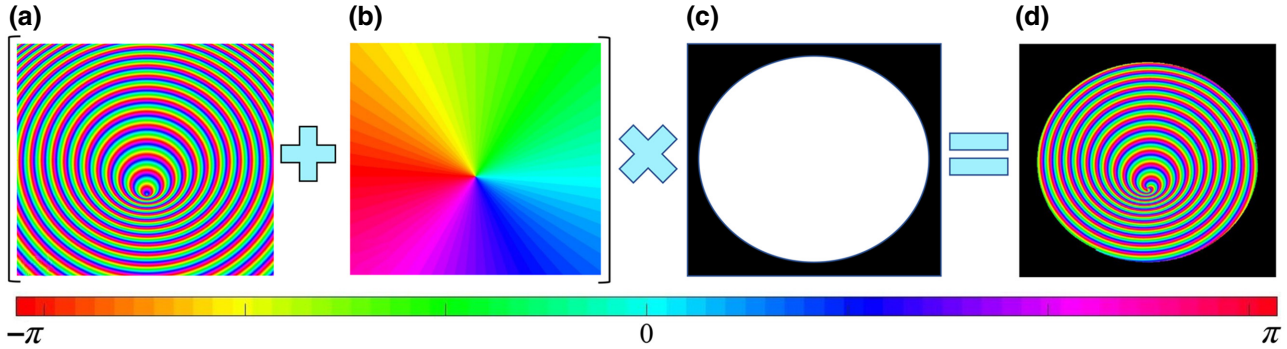

FIG. 2. Schematic diagrams of phase masks for generating the first-order Bessel-like acoustic beam: (a) zero-order Bessel-like acoustic beam phase, (b) vortex phase, (c) circular aperture, and (d) first-order Bessel-like acoustic beam phase as the radiation surface.

IV. RESULTS AND DISCUSSION

Figure 3 depicts the numerical results of a zero-order Bessel-like acoustic beam propagating along a snakelike trajectory, $f = 0$, $g = 200(1 - \cos\{\pi[(z/k) - 60]/400\})$. The center slice of the distribution of the acoustic field is simulated and the result is shown in Fig. 3(a). The intensity distribution of the acoustic field of this Bessel-like acoustic beam on the center slice of the x-z plane shows that the propagation path of the beam bends and asymptotically takes the form of a zero-order Bessel function. From the result, it is clear that the beam is self-bending. The bending of an acoustic beam in free space is the result of a particular interference pattern. It is a hybrid beam that can bend, while maintaining a diffraction-resisting circularly symmetric profile. The effective width of the beam (FWHM) is of the order of one wavelength. Its side lobe has approximately the same bending shape as that of the main lobe. Figures 3(b)–3(e) show the numerical simulations of the transverse intensity of Bessel-like acoustic beam patterns on the x-y plane taken at $z = 10$, 30, 50, and 70 mm, respectively, as marked by the dashed lines in Fig. 3(a). The white dotted lines in Figs. 3(b)–3(e) indicate that the trajectory of the acoustic beam conforms to the expression $g = 200(1 - \cos\{\pi[(z/k) - 60]/400\})$. The cross-section distribution of the beam is off-center, which is basically the same as that of the general zero-order Bessel beam. The calculated phase information is used to create a lens, as shown in Fig. 3(f).

Then, we superimpose a vortex phase [Fig. 2(b)] on the phase of the zero-order Bessel-like acoustic beam [Figs. 2(a) or 3(f)]. The obtained phase allows us to generate the first-order Bessel-like acoustic beam [Fig. 2(d)]. Figure 4(a) shows the intensity of the acoustic field of the first-order Bessel-like acoustic beam in the center slice of the x-z plane. An acoustic dark field corresponding to the minimum acoustic intensity appears on the center of the vortex axis (i.e., the axis along the beam vortex). Figures 4(b)–4(e) show the numerical simulations of the transverse intensity patterns of the first-order Bessel-like acoustic beam on the x-y plane taken at $z = 10$, 30, 50, and 70 mm, respectively, as marked by the dashed lines in Fig. 4(a). The white dotted lines indicate that the acoustic beam from the lens propagates along the vortex axis. According to Eq. (5), if there are heavy particles near the vortex, these particles can be trapped along the vortex axis, owing to the radiation force.

We check the self-healing property of the first-order Bessel-like acoustic beam. As shown in Fig. 4(g), the main lobe of the beam is blocked by a rigid ball with a diameter of 4 mm (which is much larger than the acoustic wavelength of 0.74 mm) at $z = 4$ mm. The aperture angle it removes is $\Omega = \pi/5$. In contrast with the results in Fig. 4(a), the shape of the acoustic beam remains almost constant, even when the main lobe of the beam is blocked by the obstacle, indicating that the acoustic beam has the ability to self-heal.

We simulate the intensity, phase, and radiation force field of the first-order Bessel-like acoustic beam, and the results are shown in Fig. 5. Figure 5(a) shows the intensity distribution of the acoustic field of the first-order Bessel-like acoustic beam on the x-z plane. The initial phase distribution of the first-order Bessel-like acoustic beam on

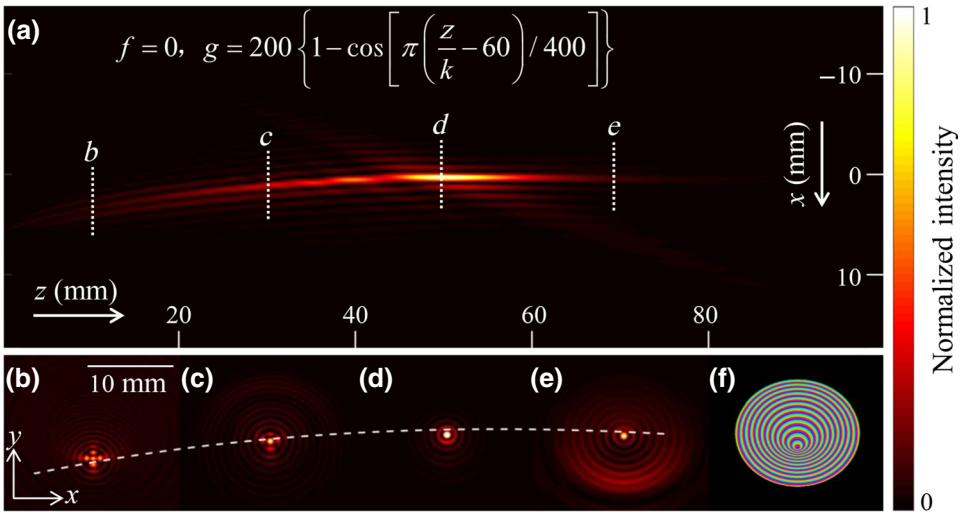

FIG. 3. Numerical simulations of a zero-order Bessel-like acoustic beam along a snakelike trajectory. (a) Intensity distribution of the acoustic field of the Bessel-like acoustic beam on the center slice of x-z plane. (b)–(e) Transverse intensity patterns of the Bessel-like acoustic beam on the x-y plane taken at $z = 10$, 30, 50, and 70 mm, respectively, marked by dashed lines in (a). White dotted line indicates that the acoustic beam from the lens propagates along a snakelike trajectory. (f) Initial phase distribution of the Bessel-like acoustic beam on the x-y plane.

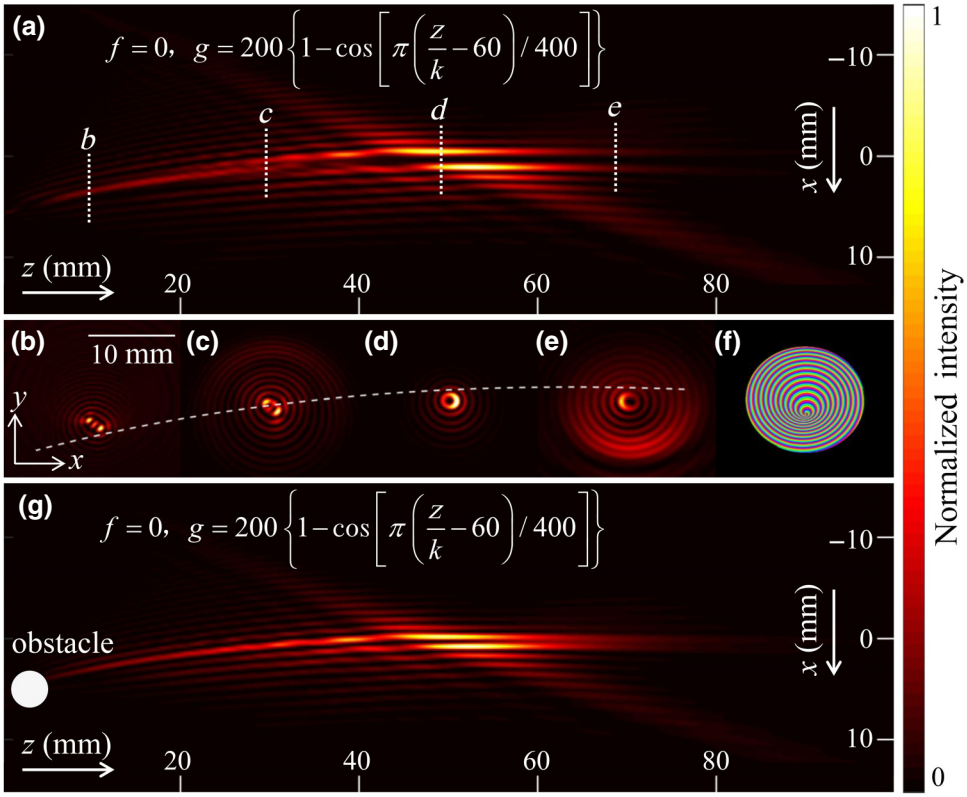

FIG. 4. (a) Numerical simulation results for the intensity distribution of the acoustic field of the first-order Bessel-like acoustic beam on the center slice of x-z plane. (b)–(e) Numerical simulations of transverse intensity of the first-order Bessel-like acoustic beam on the x-y plane taken at $z = 10$, 30, 50, and 70 mm, respectively, marked by dashed lines in (a). White dotted line indicates that the acoustic beam from the lens propagates along the vortex axis. (f) Initial phase distribution of the first-order Bessel-like acoustic beam on the x-y plane. (g) Simulation result shows the self-healing property of the first-order Bessel-like acoustic beam. Even when the main lobe of the beam is blocked by a rigid ball, the acoustic beam almost remains intact, which indicates the acoustic beam has the ability to self-heal.

the x-y plane is shown in Fig. 5(b). In the intensity distributions of the local area in Fig. 5(a) on the x-z and x-y planes [Figs. 5(c) and 5(d), respectively], an acoustic dark field corresponding to the minimum acoustic intensity appears in the center of the vortex axis, whereas the acoustic intensity is concentrated in the area surrounding the vortex axis. Therefore, a strong gradient is formed in this area. The corresponding acoustic radiation force [Figs. 5(e) and 5(f); colors and arrows indicate its magnitude and direction, respectively] points towards the vortex axis. This gives the first-order Bessel-like acoustic field its trapping capability.

To verify the simulation result, we experimentally observe the distribution of the acoustic field using Schlieren imaging, the results of which are shown in Fig. 6(a). Continuous-wave 2-MHz ultrasound is emitted from the transducer, and the lens is attached to the transducer surface and immersed in water. Two blocks of sound-absorbent rubber (width and height of 80×80 mm^2) with wedges on the surface are placed at the bottom of the tank to prevent standing waves from forming. A photograph of the absorber is shown in the bottom left of Fig. 6(a). The red dotted box marked in Fig. 6(a) is 17 mm from the transducer. Figure 6(d) is a simulation result of equal proportions of the marked white dotted box in Fig. 6(a). The experimentally observed acoustic field is generally consistent with the simulation result in Fig. 6(d). However, the intensity on both sides near the vortex axis is stronger in the experimentally observed field than in the simulation. This difference is caused by the projection integral of the acoustic intensity along the y axis. Nevertheless, the curve of the acoustic beam can be clearly distinguished using Schlieren imaging. To verify the simulation results, the acoustic field (9×9 mm^2) at $z = 50$ mm on the x-y plane is experimentally measured. The measurement interval is 0.3 mm. The measured acoustic field [Fig. 6(b)] is similar to the simulated results [Fig. 6(c)].

To experimentally verify the trapping of particles by the first-order Bessel-like acoustic beam, we position polystyrene particles (Denka, Japan) along the vortex axis, as shown in Fig. 6(e). The polystyrene particles have a nominal radius of 35 μm and a density of 1080 kg/m^3. We first add polystyrene particles to distilled water to form a suspension (0.03 g/ml). Then, this solution is injected with a low initial velocity with a dropper near the vortex axis. As shown in Fig. 6(e), a certain number of particles injected from the dropper are trapped in the vortex axis and move along a predefined trajectory. The dotted red arrows indicate the particle trajectories. The white dotted box at the bottom right of Fig. 6(e) is a partial magnification of the image, in which the curved arrangement of the particles can be observed. The bottom left inset of Fig. 6(e) shows a photograph of the acoustic lens. The initial velocity (both magnitude and direction) of the particles is not well controlled. Thus, some particles, which have an initial velocity that is too low, are unable to enter the curve, owing to the repulsive radiation force. Similarly, some particles, which

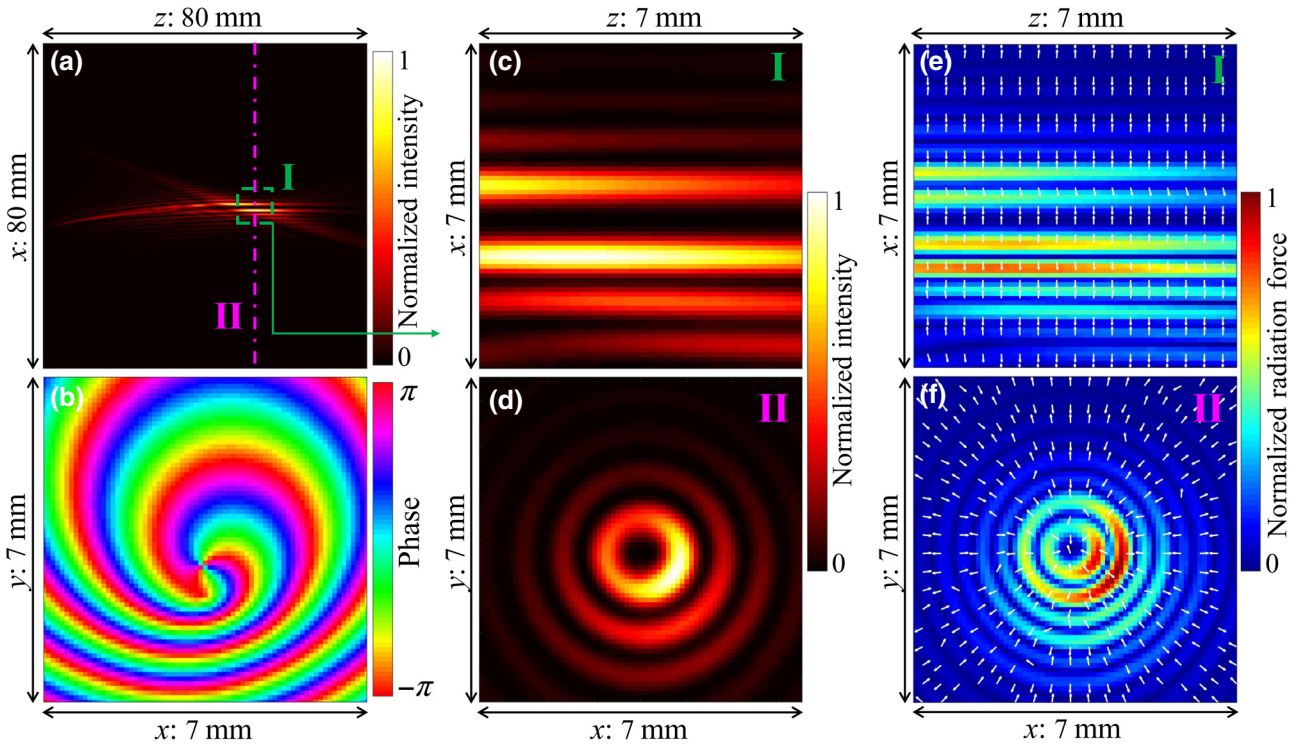

FIG. 5. (a) Numerical simulation result for the intensity distribution of the acoustic field of the first-order Bessel-like acoustic beam on the *x*-*z* plane. (b) Phase distribution of the first-order Bessel-like acoustic beam on the *x*-*y* plane. Normalized intensity of the acoustic field on (c) *x*-*z* plane and (d) *x*-*y* plane. Radiation force field on (e) *x*-*z* plane and (f) *x*-*y* plane.

have an initial velocity that is too high, cannot be trapped in the curve. In both cases, the particles are suspended elsewhere in the tank, and some are transported in parallel paths along adjacent intensity minima. The particles in the vortex axis move along the vortex axis, which is a predefined trajectory, and the transport velocity is approximately 1.57 mm/s. Both acoustic radiation force and drag force have effects on the particles' transportation. This

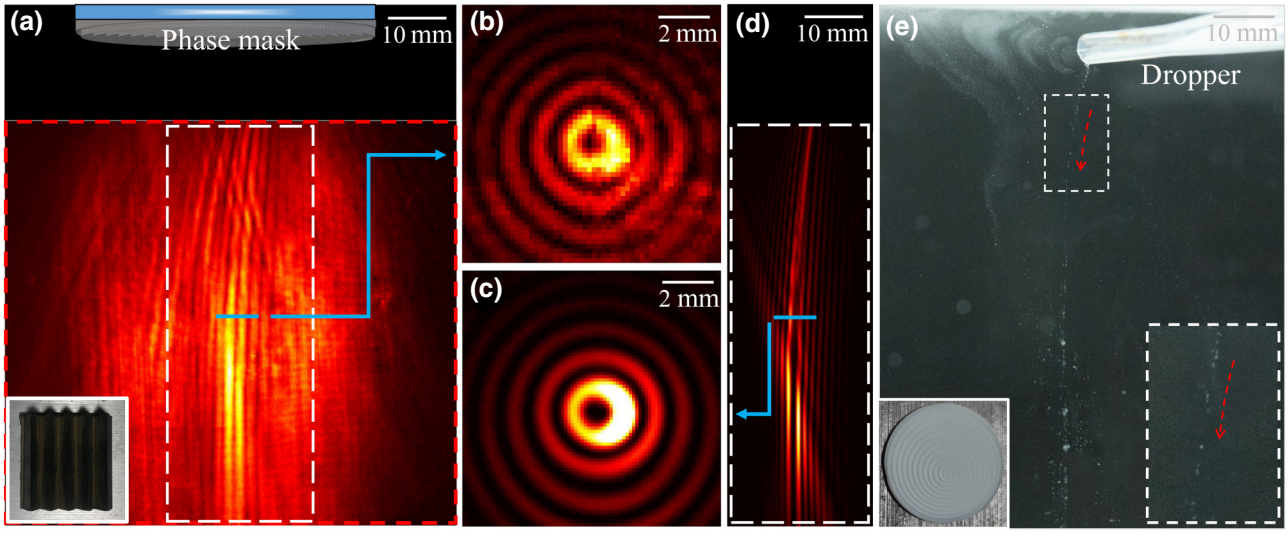

FIG. 6. (a) Experimental results of the first-order Bessel-like acoustic beam generated using an acoustic phase lens. Result is shown in red dotted box. (b) Experimental results of intensity of the acoustic field of the first-order Bessel-like acoustic beam measured by hydrophone. (c),(d) Numerical simulation results of (b),(a), respectively. (e) Experimental particle trapping using acoustic phase lens. Dotted red arrows indicate particle trajectories. White dotted box is a partial magnification of this image. White box contains a photograph of the acoustic phase lens.

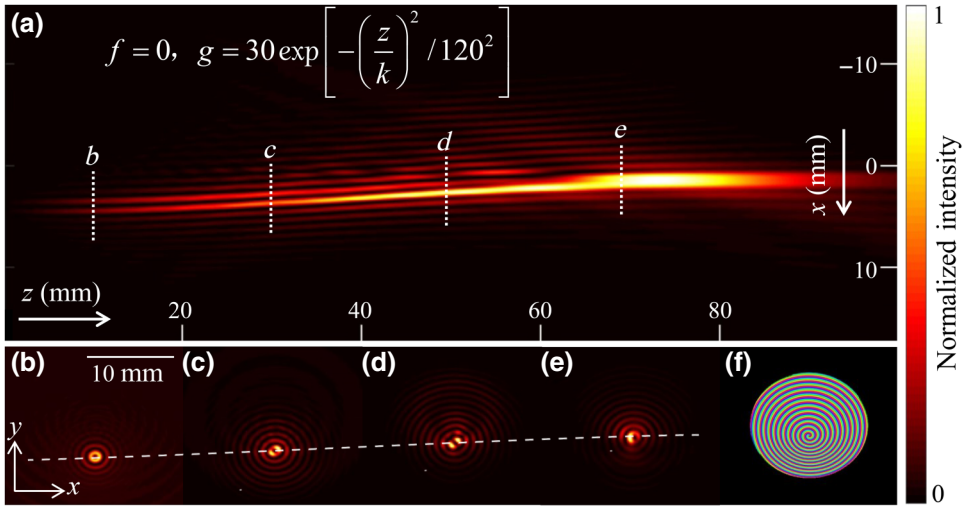

FIG. 7. Numerical simulations of a first-order Bessel-like acoustic beam along a Gaussian trajectory. (a) Intensity distribution of the acoustic field of the first-order Bessel-like acoustic beam on the center slice of x-z plane. (b)–(e) Transverse intensity of first-order Bessel-like acoustic beam patterns on x-y plane taken at $z = 10$, 30, 50, and 70 mm, respectively, marked by dashed lines in (a). White dotted line indicates that the acoustic beam from the lens propagates along the Gaussian trajectory. (f) Vortex phase distribution of the Gaussian Bessel-like acoustic beam on the x-y plane.

experiment verifies that the structure can trap particles with curved trajectories and the particles can be transported.

Following a similar procedure, we then investigate first-order Bessel-like acoustic beams with different predefined trajectories. Figure 7 depicts the numerical results of a first-order Bessel-like acoustic beam propagating along a Gaussian trajectory of $f = 0,\ g = 30\exp[-(z/k)^2/120^2]$. The center slice of the distribution of the Bessel-like acoustic field is simulated, and the result is shown in Fig. 7(a). The intensity distribution of the acoustic field of the first-order Bessel-like acoustic beam on the center slice of the x-z plane shows the bending of the propagation path of the beam. Figures 7(b)–7(e) show the numerical simulations of the transverse intensity of the first-order Bessel-like acoustic beam patterns on the x-y plane taken at $z = 10$, 30, 50, and 70 mm, respectively, as marked by the dashed lines in Fig. 7(a). The white dotted lines in Figs. 7(b)–7(e) indicate that the acoustic beam from the

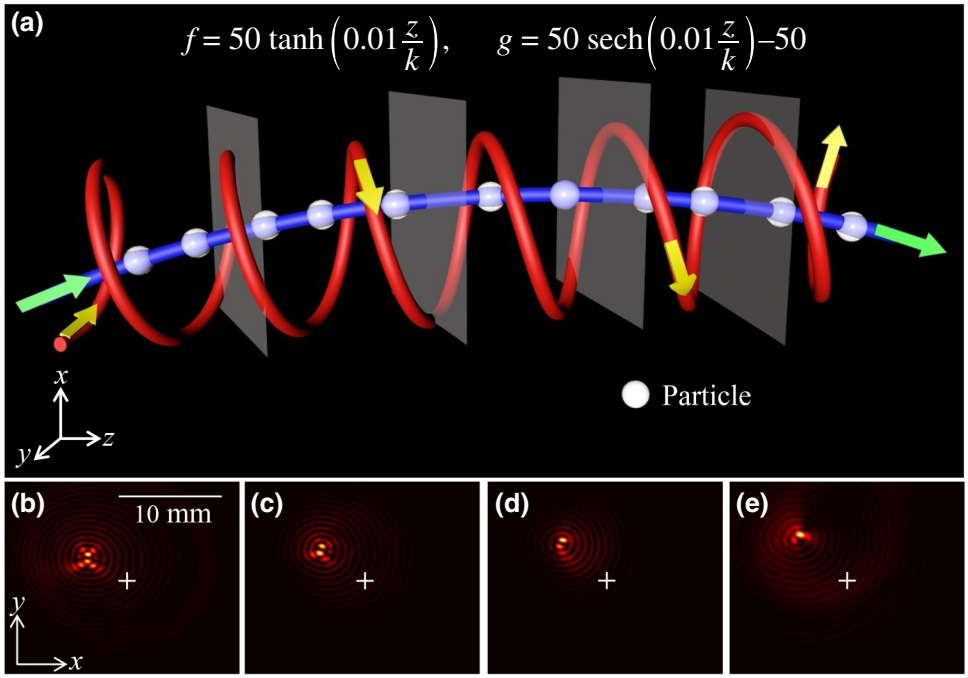

FIG. 8. Numerical simulations of a Bessel-like acoustic beam propagating along a 3D curved trajectory. (a) Schematic illustration of particle transportation along the bending trajectory. (b)–(e) Acoustic beam patterns taken at different transverse planes marked in (a). Cross marks center of the initial beam as a reference point.

lens propagates along the predefined Gaussian trajectory of $g = 30\exp[-(z/k)^2/120^2]$. The calculated initial phase information is shown in Fig. 7(f).

It should be noted that the arbitrary bending of the Bessel beam can hardly be preserved infinitely, and the fate of a Bessel beam after a long propagation distance is a straight line. This is because the bending characteristics are due to the phase change on the plate. We should pay attention to the finite size of the transducer plate in real cases, noting that an ideal Bessel beam requires an infinite wave front to facilitate its propagation. A possible approach to increase the effective bending distance of the beam is to increase the initial phase information of the acoustic source. Thus, an increase of the size of the transducer and phase plate, or an increase of the acoustic frequency with higher accuracy and more detailed phase information on the plate, should be adopted to increase the effective bending distance.

Finally, we demonstrate that the Bessel-like acoustic beams can follow 3D trajectories. In Fig. 8(a), the schematic illustration of particle transportation along the bending trajectory is shown, where the curve $[f(z), g(z), z]$ is given by $f(z) = 50\tanh[0.01(z/k)]$ and $g(z) = 50\mathrm{sech}[0.01(z/k)] - 50$. Figures 8(b)–8(e) show the simulated acoustic beam patterns on the x-y plane taken at different transverse planes marked in Fig. 8(a). The cross marks the center of the initial beam as a reference point.

V. CONCLUSION

We experimentally demonstrate self-bending Bessel-like acoustic beams that propagate along arbitrary trajectories with self-healing properties. We also demonstrate that our acoustic phase lens can be used to trap particles. This is a particular method to regulate the spatial distribution of particles with acoustic waves. The curved acoustic beams introduced in this work may be useful in applications that would benefit from the additional flexibility of arbitrary, paraxial, and 3D trajectories. The proposed acoustic lens has potential biomedical applications, such as cell transportation in a predefined trajectory and targeted drug delivery *in vivo*. We will continue to look for other ways of using diffraction-free acoustic beams to achieve particle trapping, to make acoustic particle trapping easier and more effective.

ACKNOWLEDGMENTS

This work is supported by the National Natural Science Foundation of China (Grants No. 11774263 and No. 11834008) and the National Key Research and Development Program of China (Grant No. 2016YFA0100800).

[1] J. Durnin, J. J. Miceli, and J. H. Eberly, Diffraction-Free Beams, Phys. Rev. Lett. **58**, 1499 (1987).

[2] J. W. Goodman, *Introduction to Fourier Optics* (Roberts & Company Publishers, Englewood, Colorado, USA, 2005).

[3] G. Scott and N. McArdle, Efficient generation of nearly diffraction-free beams using an axicon, Opt. Eng. **31**, 2640 (1992).

[4] J. Arlt and K. Dholakia, Generation of high-order bessel beams by use of an axicon, Opt. Commun. **177**, 297 (2000).

[5] D. McGloin and K. Dholakia, Bessel beams: Diffraction in a new light, Contemp. Phys. **46**, 15 (2005).

[6] T. Cižmar, V. Kollarova, X. Tsampoula, F. J. Gunnmoore, W. Sibbett, Z. Bouchal, and K. Dholakia, Generation of multiple bessel beams for a biophotonics workstation, Opt. Express **16**, 14024 (2008).

[7] G. Milne, G. D. M. Jeffries, and D. T. Chiu, Tunable generation of bessel beams with a fluidic axicon, Appl. Phys. Lett. **92**, 261101 (2008).

[8] I. A. Litvin, M. Mclaren, and A. Forbes, A conical wave approach to calculating bessel-gauss beam reconstruction after complex obstacles, Opt. Commun. **282**, 1078 (2009).

[9] N. Chattrapiban, E. A. Rogers, D. Cofield, W. T. Hill, and R. Roy, Generation of nondiffracting bessel beams by use of a spatial light modulator, Opt. Lett. **28**, 2183 (2003).

[10] R. Vasilyeu, A. Dudley, N. A. Khilo, and A. Forbes, Generating superpositions of higher-order bessel beams, Opt. Express **17**, 23389 (2009).

[11] A. Carbajal-Dominguez, J. Bernal, A. Martin-Ruiz, and G. M. Niconoff, Generation of J0 bessel beams with controlled spatial coherence features, Opt. Express **18**, 8400 (2010).

[12] W. Williams and J. B. Pendry, Generating bessel beams by use of localized modes, J. Opt. Soc. Am. A **22**, 992 (2005).

[13] C. Hwang, K. Kim, and B. Lee, Bessel-like beam generation by superposing multiple airy beams, Opt. Express **19**, 7356 (2011).

[14] I. Chremmos, Z. Chen, D. N. Christodoulides, and N. K. Efremidis, Bessel-like optical beams with arbitrary trajectories, Opt. Lett. **37**, 5003 (2012).

[15] J. Zhao, P. Zhang, D. Deng, J. Liu, Y. Gao, I. Chremmos, N. K. Efremidis, D. N. Christodoulides, and Z. Chen, Observation of self-accelerating bessel-like optical beams along arbitrary trajectories, Opt. Lett. **38**, 498 (2013).

[16] J. Zhao, I. Chremmos, D. Song, D. N. Christodoulides, N. K. Efremidis, and Z. Chen, Curved singular beams for three-dimensional particle manipulation, Sci. Rep. **5**, 12086 (2015).

[17] D. Baresch, J.-L. Thomas, and R. Marchiano, Observation of a Single-Beam Gradient Force Acoustical Trap for Elastic Particles: Acoustical Tweezers, Phys. Rev. Lett. **116**, 024301 (2016).

[18] D. Baresch, J.-L. Thomas, and R. Marchiano, Orbital Angular Momentum Transfer to Stably Trapped Elastic Particles in Acoustical Vortex Beams, Phys. Rev. Lett. **121**, 074301 (2018).

[19] D. Baresch and V. Garbin, Acoustic trapping of microbubbles in complex environments and controlled payload release, Proc. Natl. Acad. Sci. U. S. A. **117**, 15490 (2020).

[20] K. Melde, A. G. Mark, T. Qiu, and P. Fischer, Holograms for acoustics, Nature **537**, 518 (2016).

[21] K. Melde, E. Choi, Z. Wu, S. Palagi, T. Qiu, and P. Fischer, Acoustic fabrication via the assembly and fusion of particles, Adv. Mater. **30**, 1704507 (2018).

[22] M. A. Norasikin, D. M. Plasencia, S. Polychronopoulos, G. Memoli, Y. Tokuda, and S. Subramanian, in *the 31st Annual ACM Symposium on User Interface Software and Technology* (ACM, Berlin, Germany, 2018), p. 247.
[23] C. Rubio, D. Tarrazó-Serrano, O. V. Minin, A. Uris, and I. V. Minin, Acoustical hooks: A new subwavelength self-bending beam, Results Phys. **16**, 102921 (2020).
[24] L. Yue, O. V. Minin, Z. Wang, J. N. Monks, A. S. Shalin, and I. V. Minin, Photonic hook: A new curved light beam, Opt. Lett. **43**, 771 (2018).
[25] I. V. Minin, O. V. Minin, G. M. Katyba, N. V. Chernomyrdin, V. N. Kurlov, K. I. Zaytsev, L. Yue, Z. Wang, and D. N. Christodoulides, Experimental observation of a photonic hook, Appl. Phys. Lett. **114**, 031105 (2019).
[26] L. Cox, K. Melde, A. J. Croxford, P. Fischer, and B. W. Drinkwater, Acoustic Hologram Enhanced Phased Arrays for Ultrasonic Particle Manipulation, Phys. Rev. Appl. **12**, 064055 (2019).
[27] A. Marzo, S. A. Seah, B. W. Drinkwater, D. R. Sahoo, B. Long, and S. Subramanian, Holographic acoustic elements for manipulation of levitated objects, Nat. Commun. **6**, 8661 (2015).
[28] A. Marzo and B. W. Drinkwater, The development of dynamic holographic acoustic tweezers, J. Acoust. Soc. Am. **144**, 1896 (2018).
[29] A. Marzo and B. W. Drinkwater, Holographic acoustic tweezers, Proc. Natl. Acad. Sci. **116**, 84 (2019).
[30] A. Marzo, T. Corkett, and B. W. Drinkwater, Ultraino: An open phased-array system for narrowband airborne ultrasound transmission, IEEE Trans. Ultrason. Ferroelectr. Freq. Control **65**, 102 (2017).
[31] A. Marzo, A. Ghobrial, L. Cox, M. Caleap, A. J. Croxford, and B. W. Drinkwater, Realization of compact tractor beams using acoustic delay-lines, Appl. Phys. Lett. **110**, 014102 (2017).
[32] A. C. Franklin, A. Marzo, R. Malkin, and B. W. Drinkwater, Three-dimensional ultrasonic trapping of micro-particles in water with a simple and compact two-element transducer, Appl. Phys. Lett. **111**, 094101 (2017).
[33] T. Fushimi, T. L. Hill, A. Marzo, and B. W. Drinkwater, Nonlinear trapping stiffness of mid-air single-axis acoustic levitators, Appl. Phys. Lett. **113**, 034102 (2018).
[34] F. G. Mitri, Acoustic radiation force of high-order bessel beam standing wave tweezers on a rigid sphere, Ultrasonics **49**, 794 (2009).
[35] P. L. Marston, Axial radiation force of a bessel beam on a sphere and direction reversal of the force, J. Acoust. Soc. Am. **120**, 3518 (2006).
[36] P. L. Marston, Radiation force of a helicoidal bessel beam on a sphere, J. Acoust. Soc. Am. **125**, 3539 (2009).
[37] L. Zhang and P. L. Marston, Angular momentum flux of nonparaxial acoustic vortex beams and torques on axisymmetric objects, Phys. Rev. E **84**, 065601 (2011).
[38] L. Zhang and P. L. Marston, Geometrical interpretation of negative radiation forces of acoustical bessel beams on spheres, Phys. Rev. E **84**, 035601 (2011).
[39] L. Zhang and P. L. Marston, Axial radiation force exerted by general non-diffracting beams, J. Acoust. Soc. Am. **131**, EL329 (2012).
[40] X. Ren, Q. Zhou, Z. Xu, and X. Liu, Acoustic hook beam lens for particle trapping, Appl. Phys. Express **13**, 064003 (2020).
[41] Z. Xu, H. Chen, X. Yan, M. Qian, and Q. Cheng, Quantitative calibration of sound pressure in ultrasonic standing waves using the schlieren method, Opt. Express **25**, 20401 (2017).
[42] Z. Xu, H. Chen, X. Yan, M. Qian, and Q. Cheng, Three-dimensional reconstruction of nonplanar ultrasound fields using radon transform and the schlieren imaging method, J. Acoust. Soc. Am. **142**, 82 (2017).
[43] Q. Zhou, J. Zhang, Z. Xu, and X. Liu, Acoustic interference lens for trapping micro-scale particles, J. Phys. D: Appl. Phys. **52**, 455302 (2019).
[44] Q. Zhou, J. Zhang, X. Ren, Z. Xu, and X. Liu, Multi-bottle beam generation using acoustic holographic lens, Appl. Phys. Lett. **116**, 133502 (2020).
[45] P. B. Muller, R. Barnkob, M. J. Jensen, and H. Bruus, A numerical study of microparticle acoustophoresis driven by acoustic radiation forces and streaming-induced drag forces, Lab. Chip **12**, 4617 (2012).
[46] M. A. Abdelaziz and D. G. Grier, Acoustokinetics: Crafting force landscapes from sound waves, Phys. Rev. Res. **2**, 013172 (2020).